Backflows in Rotating Fluids Moving Axially through Expanding Cross Sections

R. W. GORE and W. E. RANZ

University of Minnesota, Minneapolis, Minnesota

Secondary backflows in swirling fluids have been reported; some are useful, but there is little scientific understanding of such phenomena. In most liquid fuel burners primary combustion air is made to swirl and fill an expanding flow cross section. A resulting backflow stabilizes combustion by recirculating hot product gases. But some backflows are not so desirable. Motion pictures of tornadoes reveal intense downward winds within the visible core having estimated velocities as high as 225 mi./hr. (*13*).

This paper concerns a preliminary study of backflows in rotating fluids moving axially through expanding cross sections. In particular it concerns conditions for existence and characteristics of such backflows.

SWIRLING FLOW IN A TUBE

Curious secondary flows are observed when swirling water is passed through a round tube of constant cross section. At low swirl ratios, that is at low values of the ratio of a characteristic tangential velocity to axial velocity, flow is forward everywhere. At higher swirl ratios however there appears a cylindrical core of backflow along the tube axis. At still higher swirl ratios the cylindrical core changes to an annular ring of backflow. Some of these phenomena were reported by Nutall in 1953 (*10*), explored further by Binnie in 1957 (*5*), and explained qualitatively, with supporting measurements, by Nissan and Bresan in 1961 (*9*). Similar backflows in a high velocity air vortex were observed by Eckert and Hartnett in 1955 (*7*).

The basis of Nissan and Bresan's explanation for axial backflow is progressive decay of tangential velocity. Where swirl is intense, centrifugal acceleration makes pressure low at the center line and high near the wall. Downstream, where viscous dissipation has weakened the swirl, pressure is relatively higher at the center line and lower at the wall. Thus decay of rotation gives rise to axial pressure gradients which, if of sufficient magnitude, drive secondary backflows.

According to Nissan and Bresan an annular regime of backflow appears to be associated with boundary layer growth. However even more complicated flows can occur, depending apparently on initial distribution of tangential velocities and tube diameter. For example in rotating water in a short, 9-in. diameter tube with two ⅜-in. tangential inlets at ½ in. from the wall, the authors have observed a central core and annular region of backflow sandwiched between two annular regions of forward flow.

There have been no theoretical solutions for reversed flows of this type, although Vaisey (*15*) has indicated the possibility of analyzing the problem by relaxation techniques. The important point to make here is that these reversed flows depend on viscous action.*

* However in a paper appearing in the December, 1962, issue of *Journal of Fluid Mechanics*, 14, part 4, T. Brooke Benjamin develops an inviscid theory of "vortex breakdown." By breakdown is meant secondary flows of the type shown in Figure 4 which appear in the leading-edge vortex formed above a delta wing. Vortex breakdown in a swirling flow in a tube is demonstrated by J. K. Harvey in the same issue. The phenomenon, as demonstrated by Harvey, is apparently the initiation stage of fully developed backflow.

SWIRLING FLOW IN CONVERGING CROSS SECTIONS

A well-defined secondary flow may arise in convergent nozzles within the boundary layer of a swirling fluid. Taylor's solution of this problem (*14*), when the main flow is a free vortex, indicates that the boundary layer is forced toward the nozzle throat by unbalanced centrifugal forces. For small nozzles almost all of the fluid passing through the throat arrives there by way of the boundary layer. Binnie and co-workers (*1, 2, 3, 4*) have reported many experiments in which swirling water, with a nearly free vortex tangential velocity distribution, was passed through convergent nozzles. Surprisingly it was found that water near the axis moved counter to a net forward flow direction. Binnie assumed that the mechanism of this backflow was the same as in tubes of constant cross section.

A secondary flow which is not explained in terms of either Taylor or Binnie's work has been treated theoretically and experimentally by Long (*8*) who considered the case of an inviscid fluid in solid body rotation moving through a tube toward a point sink on the tube axis. Since the fluid converged toward the point sink, the flow field was the same as in a converging nozzle of 180-deg. opening angle. Long found that fluid near the axis was accelerated toward the sink, while fluid near the tube wall was decelerated. This effect became more pronounced as the swirl ratio* was increased until, at a critical swirl ratio, a region of reversed flow appeared near the wall with a highly accelerated forward flow along the axis.

These are strikingly different results from those obtained by Binnie and Taylor. Binnie's relatively small nozzle with small opening angle (30 deg.) would tend to emphasize viscous wall effects much more than Long's. What is probably more important is that Binnie's experiments and Taylor's theory were for a free vortex distribution of tangential velocities, while Long's theoretical development and experiments were for rigid body rotation.

SWIRLING FLOW IN DIVERGING CROSS SECTIONS

In the literature of fluid mechanics no experiments have surveyed a wide range of operating conditions for swirling flows in divergent nozzles. Peters in his treatment of divergent flows under different conditions of inflow (*11*) reported no backflow with swirling inflow, possibly because his nozzles did not allow visual observations. Binnie and co-workers (*4*) have observed swirling flow through short divergent sections and reported no backflows.

However many evidences of secondary flows are found in applications. The combustion chamber of a gas turbine begins with a swirling device for primary air, and it is known that a toroidal vortex usually forms in the chamber (*6*). Most liquid fuel burners employ the same flow configuration in rudimentary form. In a more recent application Reed's stabilization of an inductively heated plasma

* The swirl ratio, defined as a characteristic tangential velocity divided by a characteristic axial velocity, is the inverse of the Rossby number of meteorology.

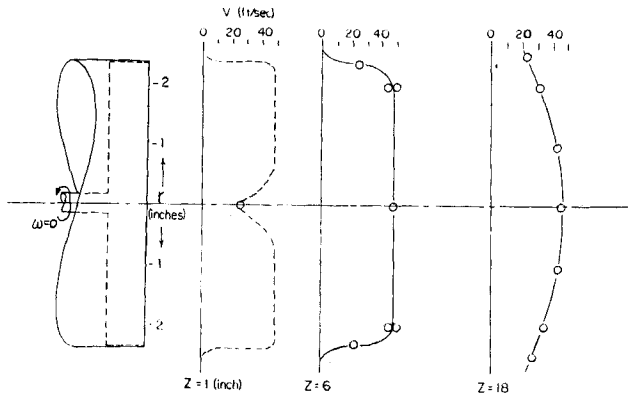

Fig. 1. Axial velocity distribution of a free jet with no rotation. ⅛-in. holes were drilled perpendicular to the swirl plate on a pattern of concentric circles. The concentric circles were spaced 3/16 in. apart, and on each circle the holes were spaced on 3/16-in. centers.

(*12*) may depend on this type of secondary flow. Secondary vortices in rotating, expanding flows are often reported in qualitative terms, but there has been no fundamental study of the characteristics of the vortex and conditions for its existence.

PRELIMINARY EXPERIMENTS: DESCRIPTION OF SECONDARY FLOWS

In the experiments reported here a number of devices were used to create nearly solid body rotation in axial flows which were then allowed to expand as free jets or pass through diverging cross sections. The most common of these was a swirl vane. Idealized, a swirl vane is a screw with more than one flight or vane, large pitch to diameter ratio, and thread depth equal to tube radius. However, because of strong secondary flows of the Taylor type radially inward on the upstream sides of vanes and separation on the downstream side, flow between vanes rotates. Outlet flow is like a rope, twisted strands of fluid from between the vanes having been twisted into a flow rope. With such a device the flow is not axisymmetric in detail, and the flow field is complicated by additional secondary flows induced by the vanes.

With the high turbulence levels of the usual swirl device backflow regions are difficult to detect. Much of the success of the experiments reported here can be attributed to a reduction of the turbulent scale and intensity.

To impart a more ideal rotation to the flow, fixed swirl plates were constructed. These were drilled with short cylindrical holes of such a number and at angles to give superficially solid body rotation and uniform axial velocity. Specifications for one such plate are given in the caption of Figure 5. It was found that angular momentum imparted by the constricting holes was larger than the angular momentum expected by a superficial tangential velocity based on hole angle. For example for another swirl plate* with outer holes drilled at 45 deg. one would expect a swirl ratio $N = v_\theta/v_z$ of unity based on a uniform superficial axial velocity. The measured swirl ratio was 2.8. The axial component of velocity in this case, while axially symmetrical, may not have been uniform. This result only emphasizes how difficult it is to realize experimentally an idealized solid body rotation in a uniform axial flow.

A motor driven perforated plate was found to be the most successful way of imparting rotation to axial flows. Holes were drilled parallel to the axis. When the plate was turned, fluid passing through the holes was carried with the plate in solid body rotation. This scheme was particularly useful in obtaining a continuous variation in angular velocity and a nearly uniform axial component of velocity. The plate described in Figure 1 was used for most of the experiments, and a sample axial velocity traverse for no rotation is shown. The dimple at the axis formed because there was no center hole where the shaft joined the swirl plate. When the swirl plate was rotated, flow downstream from the plate and very near the plate was measured with spinners and found to have the same angular velocity ω as the plate. In this case, with plate radius R and superficial velocity v_o, the swirl ratio was $N = \omega R/v_o$.

With no swirl component ($N = 0$) the free jet of air grew in cross section because surrounding air was entrained, but it grew relatively slowly. With a weak swirl component the jet expanded in cross section because of centrifugal forces. The expanding jet was roughly paraboloidal in shape, and angular velocities were observed to decrease as the flow cross section increased. There was no backflow, but center-line velocities were low compared with those of an unswirled jet.

As the swirl ratio $\omega R/v_o$ was increased beyond a value of unity, a critical condition was reached. Regions near the axis oscillated irregularly between forward flow and backflow. Smoke, introduced at the axis through hypodermic tubing, was observed to move first forward and then backward.

When the swirl ratio exceeded the critical value, the region of backflow became well defined. Figure 2 shows the flow field for a particular value of swirl ratio. In this case a toroidal vortex was found very nearly spherical in shape. The forward stagnation point was sharply defined. At this point not only was there no axial flow, but there was also no rotation. The eyes of the vortex were also well defined. The rear stagnation point was more difficult to locate. Apparently the vortex had a wake which disrupted its rear face.

When swirling fluid was expanded through a conical nozzle, a similar sequence of events was observed. At low swirl ratios there was forward flow everywhere. At a critical swirl ratio oscillations occurred. At higher swirl ratios there was always backflow. Now the flow field depended on an additional parameter, the cone angle of the confining walls.

It is interesting to contrast swirling flow and rectilinear flow through a diffuser. With no swirl and for large enough cone angles separation occurred on the wall near the throat. There was forward flow in a central jet and

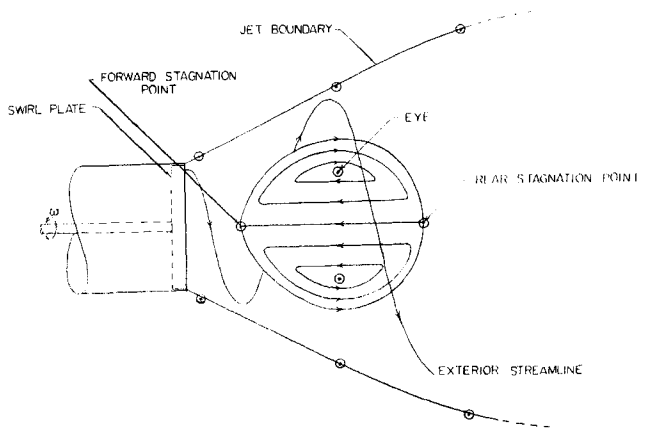

Fig. 2. Backflow in a free jet fed with a rotated fluid. (N= 1.57, R = 0.198 ft., v_o = 12.4 ft./sec.)

* Specification for this plate are given in the caption of Figure 3.

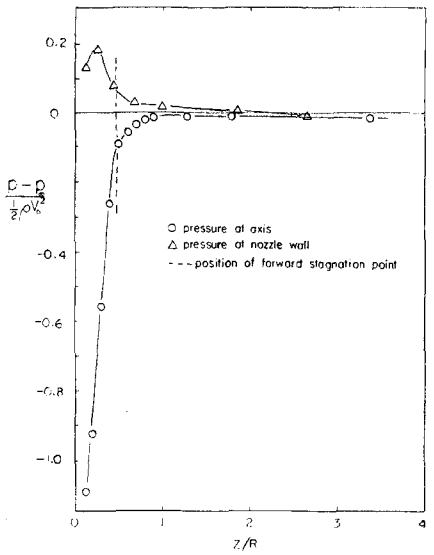

Fig. 3. Static pressure measurements at the wall and along the axis of a diverging conical nozzle. Air was rotated by a stationary swirl plate drilled with ⅛-in. slanted holes. The holes were drilled on concentric circles spaced 3/16 in. apart. Hole angle increased linearly with radial distance, the center hole being perpendicular to the plate while the outer holes were angled at 45 deg. (N = 2.8, R = 0.198 ft., v_o = 108 ft./sec., $\tan^{-1}m$ = 45 deg.)

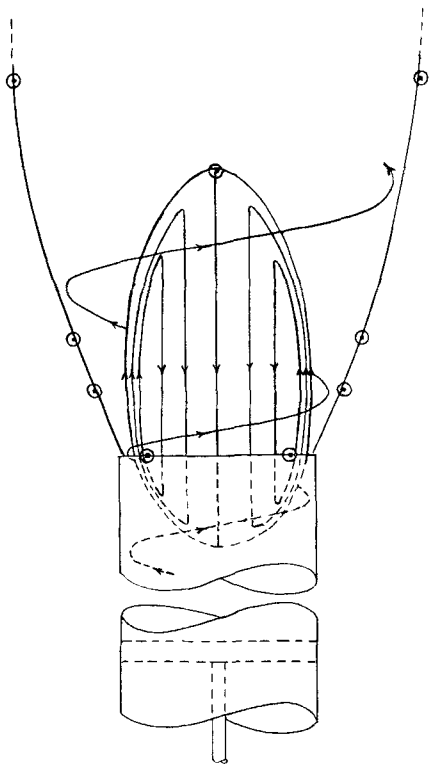

Fig. 4. Backflow in a free jet fed with rotated fluid from a recessed swirl plate. N= 4.3, R = 0.198 ft., v_o = 12.4 ft./sec.)

Fig. 5. Photograph of a gas flame held in a free air jet from a stationary swirl plate. Outer holes were angled at 45 deg. (R = 0.0833 ft., v_o = 10.4 ft./sec., fuel gas flow rate = 0.27 cu. ft./min.)

backflow along the wall. At high swirl ratios the effect was much different. Separation at the wall disappeared. Flow was accelerated near the wall and retarded or reversed along the center line. Furthermore the measured pressure distribution at the wall was such that any Taylor type of secondary flow in the boundary layer on the conical wall is a forward flow except very near the throat (see Figure 3).

Two important effects could be identified. First, axial backflow originated from axial pressure gradients created when the rotating fluid moved through increasing flow cross sections. When the swirl ratio exceeded the critical value, a pattern of reversed flow replaced these pressure gradients. Sample static pressure readings taken along the axis of a swirling jet in a 45-deg. cone are shown in Figure 3. In the region of backflow the static pressure is nearly that at an infinite distance downstream.

Second, backflow could be stopped at a stagnation point on the axis by controlling the distribution of axial velocities and pressure at some cross section upstream. This is illustrated in Figures 2 and 4 which are sketches of the flow fields of two free jets, one where a rotating swirl plate was positioned flush with the end of the tube, and one where the swirl plate was withdrawn into the tube.

With regard to similarity of the resulting flow field, swirl ratio appears to be the most important governing variable. However the basic picture was found to be modified by viscous and turbulent shear effects.

A simple evidence of backflow is shown in Figure 5. This is a photograph of a turbulent flame held in a free jet of swirling air. Fuel gas was introduced upstream along the center line. The superficial axial velocity of the air exceeded the flame velocity, and the flame was incased in air which exceeded the flame velocity everywhere except in the recirculating vortex. The direction of the flow patterns within the flame were probed with a platinum wire which had been dipped in salt solution. The characteristic bright yellow of sodium was clearly visible and indicated the presence of backflow near the axis. The flame was stable in any orientation of the burner and could be operated over a very wide capacity range.

An unsupported balloon of the size of the backflow region was found to come to rest in the flow field of Figure 2, displacing the backflow region. A considerable force was required to dislodge it from its stable position.

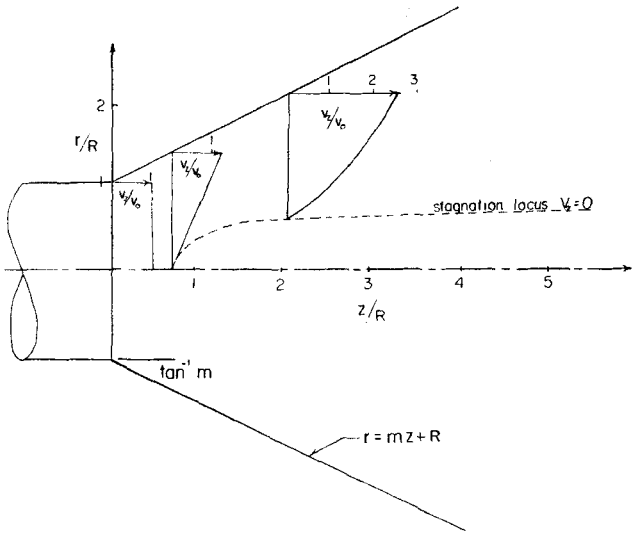

Fig. 6. Stagnation locus and axial velocities from simplified theory. ($N = 1.5$, $m = 0.5$.)

SIMPLIFIED THEORY FOR FLOW OF A ROTATING FLUID IN AN EXPANDING CROSS SECTION

Because the phenomenon described above occurs in an unbounded flow, it seems reasonable, as a first approximation, to devise a theoretical model which involves an inviscid fluid having a high degree of rotation. Consider flow in Figure 6 at which $z = 0$ has solid body rotation and expands, or is made to expand, at an angle $\tan^{-1}m$ within a conical boundary where the pressure distribution is known, for example constant pressure p_∞ .

If $o < m < 1$ and $N > 1$ sufficiently to permit a high swirl approximation,* the equations for steady state motion of an inviscid fluid in this axially symmetrical system reduce to

$$v_r \frac{\partial(rv_\theta)}{\partial r} + v_z \frac{\partial(rv_\theta)}{\partial z} = 0 \tag{1}$$

$$\frac{v_\theta^2}{r} = \frac{1}{\rho}\frac{\partial p}{\partial r} \tag{2}$$

$$v_z \frac{\partial v_r}{\partial z} = -\frac{1}{\rho}\frac{\partial p}{\partial z} \tag{3}$$

where Equations (2) and (3) are approximations. The equation of continuity is

$$\frac{1}{r}\frac{\partial(rv_r)}{\partial r} + \frac{\partial v_z}{\partial z} = 0 \tag{4}$$

Each of these equations has a helpful physical interpretation. Equation (1) expresses conservation of z-directed angular momentum. The angular momentum rv_θ may be convected in the r direction by v_r and in the z direction by v_z. Equation (2) is a balance between radial pressure gradients and radial accelerations arising from rotation. Equation (3) relates pressure gradient and velocity gradient in the z direction.

Equations (1) through (4) can be applied to a free, swirling jet which expands initially at angle $\tan^{-1}m$, where m is some function of swirl ratio N. The boundary conditions chosen are: solid body rotation at $z = 0$, that is $v_\theta = \omega r$ and $v_z = v_o$ at $z = 0$ and $r \leq R$; no flow through the conical boundary, that is $mv_z = v_r$ at $r = mz + R$; $p = p_\infty$ at $r = mz + R$ and at $z = \infty$. It should be noted that the last two boundary conditions cannot generally be imposed independently. The compatibility of these two conditions arises from the experimental observation that the boundary of a free, swirling jet is nearly conical.

An iterative procedure is now followed to obtain a flow field which has some of the important features of the observed flow. A $v_z = v_{z1}(r, z)$ is assumed. $v_r = v_r(r, z)$ is obtained from Equation (4). Substitution of v_{z1} and v_r so obtained in Equation (1) gives $v_\theta = v_\theta(r, z)$. $p(r, z)$ follows from Equation (2). A corrected $v_z = v_{z2}(r, z)$ is then obtained from Equation (3).

As a first approximation let

$$v_{z1}/v_o = 1/(1 + mz/R)^2 \tag{5}$$

that is a uniform distribution of v_z which satisfies the first boundary condition. Equation (4) gives

$$v_r/v_o = (mr/R)/(1 + mz/R)^3 \tag{6}$$

which satisfies the second boundary condition. Substitution of Equations (5) and (6) in Equation (1) results in

$$v_\theta/v_o = (Nr/R)/(1 + mz/R)^2 \tag{7}$$

which also satisfies the first boundary condition. When Equation (7) is substituted in Equation (2) and the third boundary condition is applied, the pressure distribution is indicated to be

$$\frac{p_\infty - p}{\rho v_o^2/2} = \frac{N^2}{(1 + mz/R)^2} - \frac{(Nr/R)^2}{(1 + mz/R)^4} \tag{8}$$

In Equation (8) appear axial pressure gradients resulting from the decreased swirl which is required by angular momentum conservation. Substitution of Equation (8) in Equation (3) yields a corrected v_z:

$$(v_{z2}/v_o)^2 = 1 + N^2\left[\left(1 - \frac{1}{(1 + mz/R)^4}\right)(r/R)^2 - \left(1 - \frac{1}{(1 + mz/R)^2}\right)\right] \tag{9}$$

It is interesting to inspect some of the features of the model represented by Equations (8) and (9). Because $v_{z2} = 0$ at $z = \infty$ when $N = 1$, the model predicts a critical value of unity for the swirl ratio. When $N > 1$, an axially symmetrical surface on which $v_{z2} = 0$ extends upstream toward the swirling device. The cross-sectional radius of this surface at $z = \infty$ is $R(N^2 - 1)/N^2$, and a stagnation point occur on the axis where $(1 + mz/R)^2 = N^2/(N^2 - 1)$. On Figure 6, as an example, are superimposed the locus of the stagnation surface for $N = 1.5$ and $m = 0.5$ and representative v_{z2} profiles.

At this stage of development the model does not close the surface at finite z possibly because viscous and turbulent shear have not been accounted for. Equation (9) does not give real velocities of backflow in the central region. However Equation (8) shows a pressure difference between $z = \infty$ and the stagnation point of the central region which could produce backflow velocities of the order of $v_o(N^2 - 1)^{1/2}$.

Since the stagnation pressure of flow on the axis at $z = 0$ is less than p_∞ when $N > 1$, the model suggests that backflow may penetrate to negative z. Control of the stagnation point of a real system to positive values of z appears to be dependent either on control of the pressure distribution at $z = 0$ or on the creation of a radial distribution of axial velocities at $x = 0$ so that the stagnation pressure of the flow on the axis exceeds p_∞.

CRITICAL SWIRL RATIOS, FLOW FIELDS, AND BACKFLOW VELOCITIES

A simple, constant-temperature hot wire anemometer was used for velocity measurements. Because of high damping in the Kelvin bridge balancing circuit no at-

* Detailed development of these assumptions is shown in the appendix.

tempt was made to measure turbulent fluctuations. The probe consisted of a 1 mil wire ¼ in. long which was supported on two needles. The anemometer was calibrated with a standard pitot tube and an ASTM standard nozzle. Tufts and smoke traces indicated flow directions. Small static pressure probes of standard design were also used to measure characteristics of the flow fields. Lightweight spinners of various design gave values of angular velocity. Most of these consisted of thin rods on nylon bearings carrying disk vanes at various radii.

One spinner turned on the flow axis and had two cylindrical arms at 180 deg. extending to the boundary of the flow cross section. The angular velocity of the spinner was interpreted as an average angular velocity of the cross section. Average angular velocities were observed to decrease rapidly as the flow cross section increased. In the range $0 < z < 3R$ measured values agreed quite well with Equation (7). At larger z, however, measured average angular velocities showed a plateau value greater than zero.

Another spinner had paddles to catch the wind at a short radial distance. Measurements with this spinner showed that there was no angular velocity near the axis at the forward stagnation point. At the rear stagnation point the angular velocity near the axis was found to be as much as twice the average at that point. Apparently the region near the forward stagnation point is fed by center-line fluid with only a small amount of angular momentum. As this fluid flows around the vortex, it acquires angular momentum by diffusion from the exterior fluid. As the flow converges toward the rear stagnation point, conservation of this angular momentum is evidenced by an increased angular velocity near the axis.

It was found that flow patterns were quite sensitive to disturbances created by probes. In order to minimize the relative magnitude of these disturbances most measurements were made on a large 5-in. diameter jet. Qualitative confirmation of the results obtained for the large jet was obtained in both air and water with a 1.75-in. diameter jet.

Critical swirl ratios were measured in both air and water over a range of operating conditions. At the critical swirl ratio oscillating flow reversals appeared on the axis at about $z = 3R$. It was found that critical swirl ratio was independent of Reynolds number in the range $20 < N_{Re} < 60{,}000$, where $N_{Re} = RV_o/\nu$, but that it depended on apparatus geometry.*

* In some recent work the turbulence intensity and scale of the initial flow were varied with turbulence grids which rotated with the flow and were positioned flush with the tube end. It was found that the critical swirl ratio varied from 1.2 to 2.8 as the turbulence intensity and scale were increased.

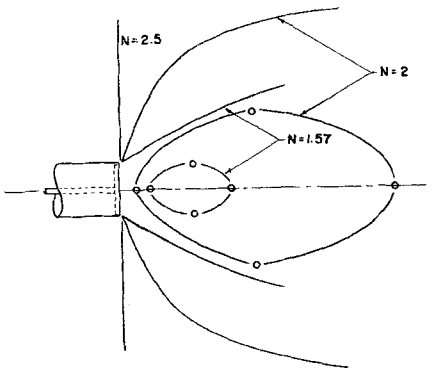

Fig. 7. Effect of swirl ratio on flow field for swirl plate positioned flush with tube end. Jet boundary and back-flow region are outlined. ($R = 0.198$ ft., $v_o = 12.4$ ft./sec.)

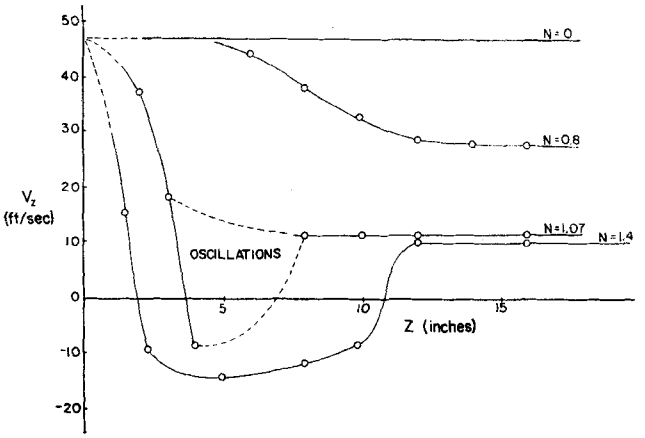

Fig. 8. Velocities along axis of free jet fed with a rotated fluid. ($R = 0.198$ ft., $v_o = 47$ ft./sec., swirl plate flush with tube end.)

Critical swirl ratio and shape of jet depended on the position of the rotated plate in the tube. When the plate was flush with the end of the tube, the critical swirl ratio was 1.36. When the plate was recessed 1 ft. into the tube, the critical swirl ratio was 1.15. The difference may have been caused by turbulence generated as fluid passed through holes in the plate. The initial scale of this turbulence was probably of the order of a hole diameter, and, in the case of a recessed plate, would have decayed before reaching the free jet. With the swirl plate at the tube end, however, this turbulence was introduced directly into the jet. Such turbulence would tend to increase momentum transfer. A higher swirl ratio would then be required to compensate for z, momentum more easily transferred to the stagnation region from large r.

With the swirl plate recessed, the region of backflow grew as N increased, and the forward stagnation point moved into the tube. A typical case is diagramed in Figure 4.* The outside shape of the jet was relatively insensitive to changes in N when $N > N_c$. It expanded at a half angle of about 20 deg. ($m = 0.364$) for swirl ratios as high as 7. Backflow velocity, measured on the axis at the mouth of the tube, increased with increasing N. When $R = 0.198$ ft. and $v_o = 12.8$ ft./sec., typical values of backflow velocity were about 12% of $v_o(N^2 - 1)^{1/2}$.

When the rotated swirl plate was positioned flush with the end of the tube, the backflow did not penetrate into the tube, and the flow field varied greatly with N. As N increased, the region of backflow grew in size and changed in shape. Finally a condition was reached where the jet expanded at right angles, and the whole region in front of the jet was in backflow.

Outlines of flow fields for $R = 0.198$ ft. and $v_o = 12.4$ ft./sec. are plotted for several swirl ratios in Figure 7. For these same flows the maximum velocity of axial backflow remained at about 3 ft./sec. as N varied from 1.4 to 2.5. Figure 8 shows a distribution of axial velocities along the axis for forward flow, unstable flow, and backflow.

CONCLUSIONS

Backflows in rotating fluids moving axially through expanding cross sections have been demonstrated. They appear when the rotation exceeds some critical value and are basically an inviscid phenomenon. Experiments described here demonstrate important features of these flows and pose problems for theoretical analysis.

* The jet boundaries indicated in Figures 2, 4, and 7 were located by smoke traces. Because the velocity dropped quite abruptly across this boundary for $Z < 6R$, tufts could be used to locate essentially the same boundary.

ACKNOWLEDGMENT

The authors are grateful to the Petroleum Research Fund for financial assistance.

NOTATION

m = tangent of half angle of flow divedgence
N = swirl ratio = $\omega R/v_o$; N_c, critical value for back-flow
p = fluid pressure, p_∞ = pressure of surroundings
r,θ,z = cylindrical coordinates
R = radius of primary flow
v_r,v_θ,v_z = fluid velocity components in cylindrical coordinates
v_o = characteristic axial velocity
ρ = fluid density
ω = angular velocity, (rad./sec.)

LITERATURE CITED

1. Binnie, A. M., and G. A. Hookings, *Proc. Roy. Soc.*, **A194**, 398 (1948).
2. Binnie, A. M., and D. P. Harris, *Quart. J. Mech. Appl. Math.*, **3**, 89 (1950).
3. Binnie, A. M., and J. D. Teare, *Proc. Roy. Soc.*, **A235**, 78 (1956).
4. Binnie, A. M., G. A. Hookings, and M. Y. M. Kamel, *J. Fluid Mech.*, **3**, 261 (1957).
5. Binnie, A. M., *Quart. J. Mech. Appl. Math.*, **10**, 276 (1957).
6. Clarke, J. S., Joint Conference on Combustion, IME and ASME, 354 (1955).
7. Eckert, E. R. G., and J. P. Hartnett, Technical Report No. 6, Heat Transfer Laboratory, University of Minnesota, Minneapolis, Minnesota (Sept., 1955).
8. Long, R. R., *Quart. J. Mech. Appl. Math.*, **9**, 385 (1956).
9. Nissan, A. H., and V. P. Bresan, *A.I.Ch.E. Journal*, **7**, 535 (1961).
10. Nuttall, J. B., *Nature*, **172**, 582 (1953).
11. Peters, H., *Natl. Advisory Comm. Aeronaut. Tech. Memo No. 737*, Washington, D. C. (1934).
12. Reed, T. B., *J. Applied Phys.*, **32**, 821 (1961).
13. Rossmann, Fritz O., "Cumulus Dynamics," Pergamon Press, New York (1960).
14. Taylor, G. I., *Quart. J. Mech.*, **3**, 129 (1950).
15. Vaisey, G., *Ninth Internatl. Cong. for Appl. Mech.*, **3**, 339 (1957).

Manuscript received December 28, 1962; revision received July 8, 1963; paper accepted July 10, 1963. Paper presented at A.I.Ch.E. Chicago meeting.

APPENDIX

In cylindrical coordinates the time-independent equations governing the flow of an inviscid, incompressible fluid with axial symmetry are the equation of continuity

$$\frac{1}{r}\frac{\partial}{\partial r}(rv_r)+\frac{\partial v_z}{\partial z}=0 \tag{1}$$

the θ component of the equation of motion

$$v_r\frac{\partial(rv_\theta)}{\partial r}+v_z\frac{\partial(rv_\theta)}{\partial z}=0 \tag{2}$$

the r component of the equation of motion

$$v_r=\frac{\partial v_r}{\partial r}+v_z\frac{\partial v_r}{\partial z}-\frac{v_\theta^2}{r}=-\frac{1}{\rho}\frac{\partial p}{\partial r} \tag{3}$$

the z component of the equation of motion

$$v_r\frac{\partial v_z}{\partial r}+v_z\frac{\partial v_z}{\partial z}=-\frac{1}{\rho}\frac{\partial p}{\partial z} \tag{4}$$

A simpler form of these equations can be obtained as an approximation when $N > 1$ and $0 < m < 1$. The equations are first put into dimensionless form by dividing each variable by a characteristic quantity. The following characteristic quantities are chosen to make the dimensionless variables of order of magnitude unity:

$$v_z^\circ=\frac{m^2V_z}{V_o}$$

$$v_\theta^\circ=\frac{v_\theta}{\omega R}$$

$$v_r^\circ=\frac{v_r}{mV_o}$$

$$z^\circ=\frac{m^2z}{R}$$

$$r^\circ=\frac{r}{mR}$$

$$p^\circ=\frac{p}{\rho\omega^2R^2}$$

Substitution of the dimensionless variables into Equations (1) to (4) leads to the following set of dimensionless equations: the equation of continuity

$$1\left(\frac{1}{r^*}\frac{\partial}{\partial r^*}r^*\,v_r^*\right)+1\left(\frac{\partial v_z^*}{\partial z^*}\right)=0 \tag{5}$$

the θ component of the equation of motion

$$1\left(v_r^*\frac{\partial r^*\,v_\theta^*}{\partial r^*}\right)+1\left(v_z^*\frac{\partial r^*\,v_\theta^*}{\partial z^*}\right)=0 \tag{6}$$

the r component of the equation of motion

$$1\left(v_r^*\frac{\partial v_r^*}{\partial r^*}\right)+1\left(v_z^*\frac{\partial v_r^*}{\partial z^*}\right)-\frac{N^2}{m^2}\left(\frac{v_\theta^{*2}}{r^*}\right)=-\frac{N^2}{m^2}\left(\frac{\partial p^*}{\partial r^*}\right) \tag{7}$$

the z component of the equation of motion

$$1\left(v_r^*\frac{\partial v_z^*}{\partial r^*}\right)+1\left(v_z^*\frac{\partial v_z^*}{\partial z^*}\right)=-N^2m^4\left(\frac{\partial p^*}{\partial z^*}\right) \tag{8}$$

If the dimensionless variables are of the order of unity, then all the terms in Equations (5) and (6) are of order unity. In Equation (7) however the dimensionless variables in the last two terms are multiplied by N^2/m^2. In the experiments reported here typical values for N and m are 2 and 0.7 respectively when the swirl plate is flush with the tube end; when the swirl plate is recessed, typical values for N range between 2 and 7, while m remains approximately constant at 0.37. In both cases N^2/m^2 is much greater than unity, and the first two terms in Equation (7) can be omitted as an approximation.

In Equation (8) the product N^2m^4 multiplies the dimensionless variables in the last term. Since for a free jet N^2m^4 is of the order of unity, in general all the terms in Equation (8) are equally important. But further simplification can be gained if Equation (8) is written for the region near the axis of symmetry. In this case the first term is small and is zero at the axis since v_r^* is zero. The simplified set of equations is

$$\frac{1}{r^*}\frac{\partial}{\partial r^*}(r^*v_r^*)+\frac{\partial v_z^*}{\partial z^*}=0$$

$$v_r^*\frac{\partial(r^*v_\theta^*)}{\partial r^*}+v_z^*\frac{\partial(r^*v_\theta^*)}{\partial z^*}=0$$

$$\frac{v_\theta^{*2}}{r^*}=\frac{\partial p^*}{\partial r^*}$$

$$v_z^*\frac{\partial v_z^*}{\partial z^*}=-N^2m^4\frac{\partial p^*}{\partial z^*}$$